

Electromagnetic wave scatterings by anisotropic metamaterials: Generalized 4×4 transfer-matrix method

Jiaming Hao and Lei Zhou*

Surface Physics Laboratory (State Key Laboratory) and Physics Department, Fudan University, Shanghai 200433, People's Republic of China

(Received 19 November 2007; revised manuscript received 30 January 2008; published 4 March 2008)

We establish a generalized 4×4 transfer-matrix method to study the scatterings of electromagnetic (EM) waves by *anisotropic* metamaterials, with incident waves taking arbitrary polarizations and propagation directions. Employing this method, we illustrate how to manipulate EM wave polarizations *freely* through reflections by metamaterials. In particular, we show that it is possible to rotate the EM wave polarization direction by an arbitrary angle using a *planar* metamaterial reflector, in contrast to the conventional Faraday effect requiring a bulk medium. Finite-difference-time-domain simulations on realistic structures are performed to verify all theoretical predictions.

DOI: [10.1103/PhysRevB.77.094201](https://doi.org/10.1103/PhysRevB.77.094201)

PACS number(s): 42.25.Ja, 42.25.Bs, 78.20.Bh, 78.20.Fm

I. INTRODUCTION

Metamaterials are artificial electromagnetic (EM) materials composed by subwavelength local resonance structures of electric and/or magnetic type, and thus possess arbitrary values of permittivity and permeability dictated by such resonance structures.¹ Many novel EM properties were predicted or discovered based on metamaterials, including the negative refraction,² the zero-refraction-index band gap,³ the super-lensing effect,⁴ etc. After realizing that the unit resonance structures of metamaterials are usually anisotropic,^{5,6} people became interested in the anisotropic properties of such new materials and revealed many intriguing phenomena in different kinds of anisotropic metamaterials.⁷⁻¹⁰

We note that many previous studies on anisotropic metamaterials considered a relatively simple situation that either the \mathbf{E} field or \mathbf{H} field of the EM wave is polarized along an optical axis of the anisotropic metamaterial.⁵⁻¹² However, generally speaking, the incident EM wave can take arbitrary polarizations and propagation directions, which are not necessarily along the optical axes of the anisotropic material. Many new exciting physics appear in the general situation. The most famous example is the double refraction, that is, a beam of light incident from air could generate two light beams inside the anisotropic medium after refraction at the interface. More recently, we reported experimental and simulation results that a specific type of anisotropic metamaterial system could be employed to manipulate the polarization state of an incident EM wave, with all kinds of polarizations (circular, elliptic, and linear) realizable via adjusting material parameters.¹³ In particular, we showed that a linearly polarized light could convert its polarization completely to the cross direction after reflection by the metamaterial slab under certain conditions.¹³ These results offer the metamaterials new applications as polarization manipulators, being complementary to the conventional methods such as using optical gratings, dichroic crystals,¹⁴ recently studied planar chiral structures,¹⁵ etc.

Theoretical calculations for such a general case are much more complicated than that for the isotropic case and for the simplified anisotropic problems.⁷⁻¹² For EM waves traveling

inside an *isotropic* media, one can always write down the wave solution as a combination of two independent modes, i.e., the *s* and *p* modes, with electric or magnetic field parallel to a prefixed planar interface. Polarizations are conserved as EM wave passes across the interface for each mode, and therefore, one can study the propagations of the two modes separately employing the standard 2×2 transfer-matrix method (TMM).^{16,17} Similarly, the 2×2 TMM was also applicable in dealing with the simplified anisotropic problems where the polarization is still conserved.⁷⁻¹² However, the same thing cannot be done in a general anisotropic problem, and thus the standard 2×2 TMM should be generalized to a 4×4 version when considering the wave transmission and/or reflection in such a situation. While formalisms were previously available for an anisotropic medium with an anisotropic $\vec{\epsilon}$ tensor,¹⁶ those formulas cannot be directly applied to the present metamaterial problems where both $\vec{\epsilon}$ and $\vec{\mu}$ could be anisotropic tensors.

The aim of the present paper is to establish a generalized 4×4 TMM to study the EM wave scatterings by layered anisotropic metamaterials and to employ this method to study the polarization manipulation effects¹³ in detail. This paper is organized in the following way. We first present the formalisms of the 4×4 TMM for an arbitrary stratified anisotropic medium in Sec. II, and then employ the method to study the EM wave scatterings by several types of anisotropic metamaterials in Sec. III, with attention mainly focused on the polarization manipulation effect. We will illustrate the ideas with three examples, namely, an anisotropic interface, a single anisotropic metamaterial slab, and a double-plate metamaterial reflector, and will perform finite-difference-time-domain (FDTD) simulations¹⁸ to verify all the conclusions drawn from the TMM calculations. We finally summarize our results in the last section.

II. COMPUTATIONAL METHODOLOGY

As shown in Fig. 1, we consider a stratified medium consisting of homogeneous but anisotropic metamaterial layers, with the *z* axis chosen normal to the interfaces. We will first study the wave propagations inside a single layer, and then

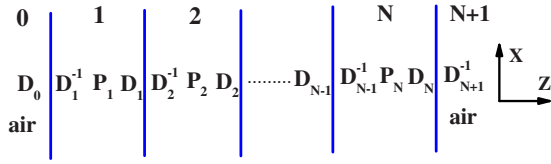


FIG. 1. (Color online) Geometry of a stratified structure consisting of N layers of anisotropic metamaterials embedded inside air.

set up a transfer matrix to connect the fields belonging to different layers, and finally derive the formulas to calculate the transmission and/or reflection coefficients.

A. Propagations of plane waves in a homogeneous anisotropic medium

We start from studying the propagations of plane waves in a homogeneous anisotropic medium, with permittivity tensor and permeability tensor given by

$$\vec{\varepsilon} = \begin{pmatrix} \varepsilon_x & 0 & 0 \\ 0 & \varepsilon_y & 0 \\ 0 & 0 & \varepsilon_z \end{pmatrix}, \quad \vec{\mu} = \begin{pmatrix} \mu_x & 0 & 0 \\ 0 & \mu_y & 0 \\ 0 & 0 & \mu_z \end{pmatrix}.$$

According to the Maxwell equations, we find the \mathbf{E} field inside such a medium to satisfy

$$\vec{k} \times [(\vec{\mu}^{-1}) \cdot (\vec{k} \times \vec{E})] + \frac{\omega^2}{c^2} \vec{\varepsilon} \cdot \vec{E} = 0, \quad (1)$$

where ω and \vec{k} denote the angular frequency and wave vector, respectively. In an explicit form, Eq. (1) can be rewritten as

$$\begin{pmatrix} (\omega/c)^2 \varepsilon_x - \mu_z^{-1} k_y^2 - \mu_y^{-1} k_z^2 & \mu_z^{-1} k_x k_y & \mu_y^{-1} k_x k_z \\ \mu_z^{-1} k_x k_y & (\omega/c)^2 \varepsilon_y - \mu_z^{-1} k_x^2 - \mu_x^{-1} k_z^2 & \mu_x^{-1} k_y k_z \\ \mu_y^{-1} k_x k_z & \mu_x^{-1} k_y k_z & (\omega/c)^2 \varepsilon_z - \mu_y^{-1} k_x^2 - \mu_x^{-1} k_y^2 \end{pmatrix} \begin{pmatrix} E_x \\ E_y \\ E_z \end{pmatrix} = 0. \quad (2)$$

In order to have nontrivial plane-wave solutions, the determinant of the matrix in Eq. (2) must vanish. With k_x and k_y prefixed and applying the constrain $\nabla \cdot (\vec{\varepsilon} \cdot \vec{E}) = 0$, we get the following equation:

$$\begin{aligned} & \left(\frac{\omega}{c} \right)^4 \varepsilon_x \varepsilon_y \varepsilon_z - \left(\sum_{i \neq j \neq l} \varepsilon_i (\varepsilon_j \mu_j^{-1} + \varepsilon_l \mu_l^{-1}) k_i^2 \right) \left(\frac{\omega}{c} \right)^2 \\ & + \left(\frac{1}{2} \sum_{i \neq j \neq l} \mu_i^{-1} \mu_j^{-1} k_l^2 \right) \sum_i \varepsilon_i k_i^2 = 0 \end{aligned} \quad (3)$$

to determine the dispersion relation between ω and k_z , where $i, j, l = x, y, z$. Equation (3) has four roots, denoted by $\{k_{z1}, k_{z2} = -k_{z1}, k_{z3}, k_{z4} = -k_{z3}\}$ and corresponding to two independent modes propagating forwardly and backwardly. For

each solution, we get the electric field distribution through solving Eq. (2) with the solution of k_z inserted. In general, the wave solution inside the anisotropic medium must be a linear combination of these four modes, so that the EM fields can be written as

$$\vec{E}(\vec{r}, t) = \sum_{\sigma=1}^4 E_{\sigma} \hat{e}_{\sigma} e^{-i[k_x x + k_y y + k_{z\sigma} z - \omega t]}, \quad (4)$$

where E_{σ} are the expansion coefficients and \hat{e}_{σ} are the \mathbf{E} -field unit vectors given by

$$\hat{e}_{\sigma} = (X_{\sigma}^2 + 1 + Z_{\sigma}^2)^{-1/2} (X_{\sigma} \hat{x} + \hat{y} + Z_{\sigma} \hat{z}), \quad (5)$$

and

$$X_{\sigma} = \frac{\mu_x^{-1} \mu_y^{-1} k_x k_y k_{z\sigma}^2 - \mu_z^{-1} k_x k_y [(\omega/c)^2 \varepsilon_z - \mu_y^{-1} k_x^2 - \mu_x^{-1} k_y^2]}{[(\omega/c)^2 \varepsilon_x - \mu_z^{-1} k_y^2 - \mu_y^{-1} k_{z\sigma}^2][(\omega/c)^2 \varepsilon_z - \mu_y^{-1} k_x^2 - \mu_x^{-1} k_y^2] - (\mu_y^{-1})^2 k_x^2 k_{z\sigma}^2}, \quad (6)$$

$$Z_{\sigma} = \frac{\mu_y^{-1} \mu_z^{-1} k_x^2 k_y k_{z\sigma} - \mu_x^{-1} k_y k_{z\sigma} [(\omega/c)^2 \varepsilon_x - \mu_z^{-1} k_y^2 - \mu_y^{-1} k_{z\sigma}^2]}{[(\omega/c)^2 \varepsilon_x - \mu_z^{-1} k_y^2 - \mu_y^{-1} k_{z\sigma}^2][(\omega/c)^2 \varepsilon_z - \mu_y^{-1} k_x^2 - \mu_x^{-1} k_y^2] - (\mu_y^{-1})^2 k_x^2 k_{z\sigma}^2}. \quad (7)$$

The \mathbf{H} field is easily obtained from the Maxwell equations as

$$\vec{H}(\vec{r}, t) = \sum_{\sigma=1}^4 E_{\sigma} \hat{h}_{\sigma} e^{-i[k_x x + k_y y + k_z z - \omega t]}, \quad (8)$$

where

$$\hat{h}_{\sigma} = \frac{1}{\omega} \vec{\mu}^{-1} \cdot (\vec{k} \times \hat{e}_{\sigma}). \quad (9)$$

We note that \hat{h}_{σ} are not necessarily unit vectors.

B. 4×4 transfer matrix

We now impose the boundary conditions to get a transfer matrix. The EM waves in the n th layer are expressed as

$$\begin{pmatrix} \vec{E}^{(n)} \\ \vec{H}^{(n)} \end{pmatrix} = \sum_{\sigma=1}^4 E_{\sigma}^{(n)} \begin{pmatrix} \hat{e}_{\sigma}^{(n)} \\ \hat{h}_{\sigma}^{(n)} \end{pmatrix} e^{-i[k_x x + k_y y + k_z^{(n)}(z - z_n) - \omega t]}, \quad (10)$$

where $\{E_1^{(n)}, E_2^{(n)}, E_3^{(n)}, E_4^{(n)}\}$ is a set of expansion coefficients to be determined, $\hat{e}_{\sigma}^{(n)}$, $\hat{h}_{\sigma}^{(n)}$, and $k_z^{(n)}$ are the field vectors and wave vectors calculated in the n th layer, and z_n is the starting position of the n th layer. Imposing the condition that the tangential components of \vec{E} and \vec{H} should be continuous at the boundary $z = z_{n+1}$, we find that

$$\begin{aligned} \sum_{\sigma=1}^4 E_{\sigma}^{(n)} \hat{e}_{\sigma}^{(n)} \cdot \hat{y} e^{-ik_z^{(n)} d_n} &= \sum_{\sigma=1}^4 E_{\sigma}^{(n+1)} \hat{e}_{\sigma}^{(n+1)} \cdot \hat{y} \\ \sum_{\sigma=1}^4 E_{\sigma}^{(n)} \hat{h}_{\sigma}^{(n)} \cdot \hat{x} e^{-ik_z^{(n)} d_n} &= \sum_{\sigma=1}^4 E_{\sigma}^{(n+1)} \hat{h}_{\sigma}^{(n+1)} \cdot \hat{x} \\ \sum_{\sigma=1}^4 E_{\sigma}^{(n)} \hat{h}_{\sigma}^{(n)} \cdot \hat{y} e^{-ik_z^{(n)} d_n} &= \sum_{\sigma=1}^4 E_{\sigma}^{(n+1)} \hat{h}_{\sigma}^{(n+1)} \cdot \hat{y} \\ \sum_{\sigma=1}^4 E_{\sigma}^{(n)} \hat{e}_{\sigma}^{(n)} \cdot \hat{x} e^{-ik_z^{(n)} d_n} &= \sum_{\sigma=1}^4 E_{\sigma}^{(n+1)} \hat{e}_{\sigma}^{(n+1)} \cdot \hat{x} \end{aligned} \quad (11)$$

where $d_n = z_{n+1} - z_n$. Equations (11) can be simplified as a matrix equation,

$$\begin{pmatrix} E_1^{(n+1)} \\ E_2^{(n+1)} \\ E_3^{(n+1)} \\ E_4^{(n+1)} \end{pmatrix} = D_{n+1}^{-1} D_n P_n \begin{pmatrix} E_1^{(n)} \\ E_2^{(n)} \\ E_3^{(n)} \\ E_4^{(n)} \end{pmatrix} = M_{n+1, n} P_n \begin{pmatrix} E_1^{(n)} \\ E_2^{(n)} \\ E_3^{(n)} \\ E_4^{(n)} \end{pmatrix}, \quad (12)$$

with

$$D_n = \begin{pmatrix} \hat{e}_1^{(n)} \cdot \hat{y} & \hat{e}_2^{(n)} \cdot \hat{y} & \hat{e}_3^{(n)} \cdot \hat{y} & \hat{e}_4^{(n)} \cdot \hat{y} \\ \hat{h}_1^{(n)} \cdot \hat{x} & \hat{h}_2^{(n)} \cdot \hat{x} & \hat{h}_3^{(n)} \cdot \hat{x} & \hat{h}_4^{(n)} \cdot \hat{x} \\ \hat{h}_1^{(n)} \cdot \hat{y} & \hat{h}_2^{(n)} \cdot \hat{y} & \hat{h}_3^{(n)} \cdot \hat{y} & \hat{h}_4^{(n)} \cdot \hat{y} \\ \hat{e}_1^{(n)} \cdot \hat{x} & \hat{e}_2^{(n)} \cdot \hat{x} & \hat{e}_3^{(n)} \cdot \hat{x} & \hat{e}_4^{(n)} \cdot \hat{x} \end{pmatrix}, \quad (13)$$

and

$$P_n = \begin{pmatrix} e^{-ik_z^{(n)} d_n} & & & \\ & e^{-ik_z^{(n)} d_n} & & \\ & & e^{-ik_z^{(n)} d_n} & \\ & & & e^{-ik_z^{(n)} d_n} \end{pmatrix}. \quad (14)$$

We note that in the absence of magnetic anisotropy (i.e., $\mu_x = \mu_y = \mu_z = \mu$), matrices D_n and P_n recover the results obtained previously [Eqs. (17) and (18) in Ref. 16]. When both the magnetic and electric anisotropies are absent (i.e., $\mu_x = \mu_y = \mu_z = \mu$ and $\varepsilon_x = \varepsilon_y = \varepsilon_z = \varepsilon$), the 4×4 transfer matrix $M_{n+1, n}$ is reduced to two independent 2×2 transfer matrices, recovering the isotropic medium case (see the Appendix). P_n is the usual propagation matrix to describe how EM wave propagates in the n th anisotropic layer (with a distance d_n). According to Eq. (12), we find that expansion coefficients in an arbitrary layer (say, the n th layer) can be related to those in the first layer via applying Eq. (12) iteratively,

$$\begin{pmatrix} E_1^{(n)} \\ E_2^{(n)} \\ E_3^{(n)} \\ E_4^{(n)} \end{pmatrix} = M_{n, n-1} P_{n-1} M_{n-1, n-2} P_{n-2} \cdots M_{2, 1} P_1 \begin{pmatrix} E_1^{(1)} \\ E_2^{(1)} \\ E_3^{(1)} \\ E_4^{(1)} \end{pmatrix}, \quad (15)$$

and the EM fields in the n th layer can be calculated from Eq. (10) after the expansion coefficients are known.

C. Transmission and reflection coefficients

With the transfer-matrix technique presented above, we can study both the photonic band structures and the scattering problems for any layered system consisting of anisotropic metamaterials. To calculate the band structure, one needs to diagonalize the transfer matrix calculated across a unit cell to get the Bloch wave vectors. The calculations for the transmission and/or reflection coefficients are a bit complicated, and we describe the main calculation procedures in what follows.

Suppose the system consists of N layers of anisotropic metamaterials, embedded inside an isotropic homogeneous reference medium (say, air). We label the semi-infinite reference medium on the left (right) hand side of the system as the zeroth [($N+1$)th] layer (see Fig. 1). Assume a light is incident from the zeroth layer and we want to calculate the reflected waves in this layer and the transmitted wave in the last layer. Apparently, the eigenmodes in the reference medium are just the conventional s and p modes that we defined for the isotropic medium (see the Appendix). Let $E_s^i, E_p^i, E_s^r, E_p^r$, and E_s^t, E_p^t denote the complex amplitudes of the s and p modes of the incident, reflected, and transmitted waves, respectively. Applying the techniques described previously, we relate the field inside the last layer (determined by the parameters E_s^i and E_p^i) to those inside the zeroth layer (determined by the parameters E_s^r, E_s^t, E_p^r , and E_p^t) by a transfer matrix as

$$\begin{pmatrix} E_s^t \\ 0 \\ E_p^t \\ 0 \end{pmatrix} = Q \begin{pmatrix} E_s^i \\ E_s^r \\ E_p^i \\ E_p^r \end{pmatrix} = \begin{pmatrix} Q_{11} & Q_{12} & Q_{13} & Q_{14} \\ Q_{21} & Q_{22} & Q_{23} & Q_{24} \\ Q_{31} & Q_{32} & Q_{33} & Q_{34} \\ Q_{41} & Q_{42} & Q_{43} & Q_{44} \end{pmatrix} \begin{pmatrix} E_s^i \\ E_s^r \\ E_p^i \\ E_p^r \end{pmatrix}, \quad (16)$$

where

$$Q = M_{N+1,N} P_N M_{N,N-1} P_{N-1} \cdots M_{2,1} P_1 M_{1,0} P_0. \quad (17)$$

The reflection and transmission coefficients can then be calculated as

$$r_{ss} = \left. \frac{E_s^r}{E_s^i} \right|_{E_p^i=0} = \frac{Q_{24}Q_{41} - Q_{21}Q_{44}}{Q_{22}Q_{44} - Q_{24}Q_{42}}, \quad (18)$$

$$r_{sp} = \left. \frac{E_p^r}{E_s^i} \right|_{E_p^i=0} = \frac{Q_{21}Q_{42} - Q_{22}Q_{41}}{Q_{22}Q_{44} - Q_{24}Q_{42}}, \quad (19)$$

$$\begin{aligned} t_{ss} &= \left. \frac{E_s^t}{E_s^i} \right|_{E_p^i=0} = Q_{11} \\ &+ \frac{Q_{12}(Q_{24}Q_{41} - Q_{21}Q_{44}) + Q_{14}(Q_{21}Q_{42} - Q_{22}Q_{41})}{Q_{22}Q_{44} - Q_{24}Q_{42}}, \end{aligned} \quad (20)$$

$$\begin{aligned} t_{sp} &= \left. \frac{E_p^t}{E_s^i} \right|_{E_p^i=0} = Q_{31} \\ &+ \frac{Q_{32}(Q_{24}Q_{41} - Q_{21}Q_{44}) + Q_{34}(Q_{21}Q_{42} - Q_{22}Q_{41})}{Q_{22}Q_{44} - Q_{24}Q_{42}}, \end{aligned} \quad (21)$$

$$r_{ps} = \left. \frac{E_s^r}{E_p^i} \right|_{E_s^i=0} = \frac{Q_{24}Q_{43} - Q_{23}Q_{44}}{Q_{22}Q_{44} - Q_{24}Q_{42}}, \quad (22)$$

$$r_{pp} = \left. \frac{E_p^r}{E_p^i} \right|_{E_s^i=0} = \frac{Q_{23}Q_{42} - Q_{22}Q_{43}}{Q_{22}Q_{44} - Q_{24}Q_{42}}, \quad (23)$$

$$\begin{aligned} t_{ps} &= \left. \frac{E_s^t}{E_p^i} \right|_{E_s^i=0} = Q_{13} \\ &+ \frac{Q_{12}(Q_{24}Q_{43} - Q_{23}Q_{44}) + Q_{14}(Q_{23}Q_{42} - Q_{22}Q_{43})}{Q_{22}Q_{44} - Q_{24}Q_{42}}, \end{aligned} \quad (24)$$

$$\begin{aligned} t_{pp} &= \left. \frac{E_p^t}{E_p^i} \right|_{E_s^i=0} = Q_{33} \\ &+ \frac{Q_{32}(Q_{24}Q_{43} - Q_{23}Q_{44}) + Q_{34}(Q_{23}Q_{42} - Q_{22}Q_{43})}{Q_{22}Q_{44} - Q_{24}Q_{42}}. \end{aligned} \quad (25)$$

Here, r_{ss} and r_{pp} are the *direct* reflection coefficients measur-

ing the reflected waves with polarizations conserved, whereas r_{sp} and r_{ps} are the cross-reflection coefficients denoting the reflected waves with polarizations converted. Similarly, t_{ss} and t_{pp} are the *direct* transmission coefficients, while t_{sp} and t_{ps} denote the cross-transmission coefficients. In the absence of anisotropy where Q matrix is block diagonalized (i.e., $Q_{13}=Q_{14}=Q_{23}=Q_{24}=Q_{31}=Q_{41}=Q_{32}=Q_{42}=0$), we find the polarization-converted terms become exactly zero, $r_{sp}=r_{ps}=t_{sp}=t_{ps}=0$, and the polarization-conserved coefficients recover those derived for the isotropic case¹⁹

$$r_{ss} = -Q_{21}/Q_{22}, \quad (26)$$

$$t_{ss} = Q_{11} - Q_{12}Q_{21}/Q_{22}. \quad (27)$$

The analytical forms of the coefficients defined in Eqs. (18)–(25) are usually too complicated to derive for an arbitrary anisotropic layered system, so that one needs to perform numerical computations.

III. APPLICATIONS OF THE GENERALIZED 4×4 TRANSFER-MATRIX METHOD

We now apply the method to study the EM wave scatterings in three different cases, with main attention focused on the polarization manipulation phenomena.

A. Scattering by an interface between air and anisotropic metamaterial

We first study the EM wave scatterings by an interface between air and the anisotropic metamaterial. Although the assumption of a semi-infinite sample is not quite realistic, this is the simplest model to study which yields several analytical results, from which many physical insights can be gained. Unlike the reflection by an isotropic interface which conserves the polarization, here in the presence of anisotropy, an incident wave with a definite polarization could generate a reflected wave with another polarization because of the fact $r_{sp}, r_{ps} \neq 0$. Let us define a polarization conversion ratio (PCR) as

$$\text{PCR} = r_{sp}^2 / (r_{ss}^2 + r_{sp}^2), \quad (28)$$

which measures the energy portion transformed from the original polarization, assumed as the s polarization for definiteness, to the other polarization (p polarization) after reflection. Obviously, this ratio depends on the direction (θ, ϕ) of the incident wave vector \vec{k}_{in} , which is given by $\vec{k}_{in} = (\omega/c)[\sin \theta \cos \phi \hat{x} + \sin \theta \sin \phi \hat{y} + \cos \theta \hat{z}]$.

Consider first the normal incidence case ($\theta=0^\circ$), which can be solved analytically. While ϕ is meaningless to define the direction of \vec{k}_{in} in this case, it is still meaningful to differentiate two polarizations. In consistency with the $\theta \neq 0^\circ$ case,²⁰ we define that the s -polarized wave has $\vec{E} \parallel \hat{e}_s = (-\sin \phi \hat{x} + \cos \phi \hat{y})$ and the p -polarized one has $\vec{E} \parallel \hat{e}_p = (\cos \phi \hat{x} + \sin \phi \hat{y})$ in the $\theta=0^\circ$ case. Straightforward calculations yield that

$$r_{sp} = \frac{(\sqrt{\varepsilon_x}\sqrt{\mu_x} - \sqrt{\varepsilon_y}\sqrt{\mu_y})\sin(2\phi)}{(\sqrt{\varepsilon_y} + \sqrt{\mu_x})(\sqrt{\varepsilon_x} + \sqrt{\mu_y})}, \quad (29)$$

$$r_{ss} = \frac{\sqrt{\mu_x}\sqrt{\mu_y} - \sqrt{\varepsilon_x}\sqrt{\varepsilon_y} + (\sqrt{\varepsilon_x}\sqrt{\mu_x} - \sqrt{\varepsilon_y}\sqrt{\mu_y})\cos(2\phi)}{(\sqrt{\varepsilon_y} + \sqrt{\mu_x})(\sqrt{\varepsilon_x} + \sqrt{\mu_y})}, \quad (30)$$

$$\text{PCR} = \frac{(\sqrt{\varepsilon_y}\sqrt{\mu_y} - \sqrt{\varepsilon_x}\sqrt{\mu_x})^2 \sin^2(2\phi)}{(\sqrt{\varepsilon_y}\sqrt{\mu_y} - \sqrt{\varepsilon_x}\sqrt{\mu_x})^2 + (\sqrt{\mu_x}\sqrt{\mu_y} - \sqrt{\varepsilon_x}\sqrt{\varepsilon_y})^2 - 2(\sqrt{\varepsilon_y}\sqrt{\mu_y} - \sqrt{\varepsilon_x}\sqrt{\mu_x})(\sqrt{\mu_x}\sqrt{\mu_y} - \sqrt{\varepsilon_x}\sqrt{\varepsilon_y})\cos(2\phi)}. \quad (31)$$

Analyzing Eqs. (29)–(31) provides us several interesting conclusions. First, we note that all these quantities only depend on ε_x , ε_y , μ_x , and μ_y , but have nothing to do with ε_z and μ_z since here we study the normal incidence situation. Second, we find that the polarization conversion effect disappears ($r_{sp} \equiv 0$) in the absence of anisotropy ($\mu_x = \mu_y = \mu$ and $\varepsilon_x = \varepsilon_y = \varepsilon$), and the reflection coefficient becomes

$$r_{ss} = \frac{\sqrt{\mu/\varepsilon} - 1}{\sqrt{\mu/\varepsilon} + 1}, \quad (32)$$

recovering the standard result for an isotropic case.¹⁴

With the anisotropy tuned on, r_{sp} could take a nonzero value, but the polarization conversion effect is strongly dependent on the parameter ϕ . When $\phi=0^\circ$ or $\phi=90^\circ$, we get rigorously that $r_{sp} \equiv 0$ indicating that the polarization conversion effect vanishes. This is reasonable since both \mathbf{E} and \mathbf{H} fields of the incident wave are *parallel* to a coordinate axis so that the EM wave cannot detect the anisotropy of the medium. Meanwhile, the polarization-converted reflectance $|r_{sp}|^2$ is maximized when $\phi=45^\circ$. However, a complete polarization conversion (i.e., PCR=1) does not necessarily appear at $\phi=45^\circ$ since the polarization-conserved reflectance $|r_{ss}|^2$ is also a function of ϕ . Recalling the definition of PCR in Eq. (28), we find that realizing PCR=1 requires that $r_{ss} = 0$, leading to the following condition:

$$\cos(2\phi) = \frac{\sqrt{\mu_x}\sqrt{\mu_y} - \sqrt{\varepsilon_x}\sqrt{\varepsilon_y}}{\sqrt{\varepsilon_y}\sqrt{\mu_y} - \sqrt{\varepsilon_x}\sqrt{\mu_x}}. \quad (33)$$

Equation (33) shows that, for any value of ϕ , we can always choose appropriate material constants ε_x , ε_y , μ_x , and μ_y to achieve a complete polarization conversion effect.

We now perform numerical calculations to illustrate the above analytical results. Since all metamaterials are intrinsically frequency dispersive, we assume the metamaterial under study to have the following typical response functions:

$$\mu_x = 1 + \frac{70}{12.71^2 - f^2}, \quad \mu_y = 1 + \frac{22}{6.80^2 - f^2},$$

$$\varepsilon_x = \varepsilon_y = \varepsilon_z = \mu_z = 1, \quad (34)$$

where f is the linear frequency measured in gigahertz.²¹ The calculated results of r_{sp}^2 , r_{ss}^2 , and PCR are shown in Figs. 2(a)–2(c) as functions of frequency calculated with different

values of ϕ . We generally find that the reflectances (both r_{sp}^2 and r_{ss}^2) are significantly enhanced around the two resonance frequencies [6.8 and 12.71 GHz, see Eq. (34)], and the polarization-converted reflectance r_{sp}^2 is the largest at $\phi=45^\circ$, in consistency with our above theoretical analysis. An interesting observation is that while the PCR can reach 1 at some particular frequencies for $\phi=45^\circ$ and 75° , the same is *not* true for $\phi=5^\circ$ and 15° . To understand this point, we put the frequency-dependent forms of ε_x , ε_y , μ_x , and μ_y [Eq. (34)] into Eq. (33) to calculate the value of ϕ at which a complete polarization conversion effect is realized and depicted the curve $\phi \sim f$ in Fig. 3. Indeed, for the model adopted here, we only have a specific regime of polarization angle (21° – 76°) inside which a complete polarization con-

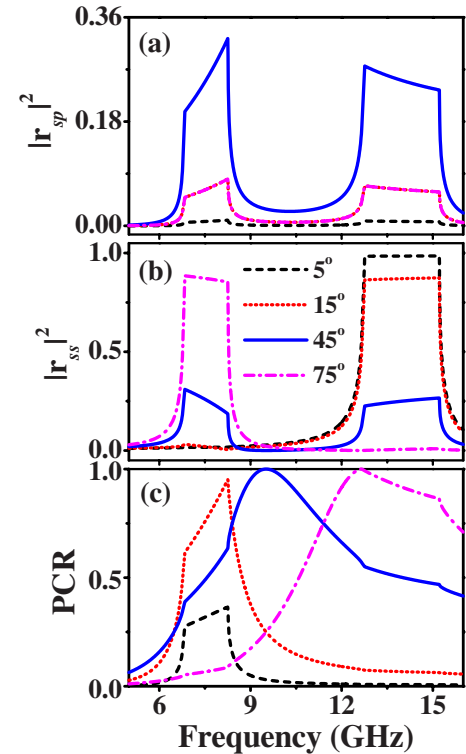


FIG. 2. (Color online) r_{sp}^2 , r_{ss}^2 , and PCR as functions of frequency for different values of ϕ , when EM waves are incident from air on the surface of a semi-infinite anisotropic metamaterial medium.

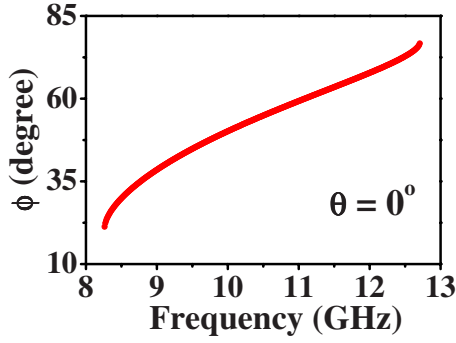


FIG. 3. (Color online) Relation between the polarization angle ϕ and frequency f , at which a complete polarization conversion effect (PCR=1) is realizable for the single-interface model.

version effect is realizable via adjusting frequency.

We turn to study the oblique incidence case, which is much more complex. Figure 4(a) shows the calculated PCR as a function of f and ϕ , with θ fixed as $\theta=15^\circ$. We note that the trajectory connecting those maximum PCR points looks very similar to the $\phi \sim f$ curve, as shown in Fig. 3, which is calculated in the normal incidence case. The physics is that both of them are dictated by the frequency dispersion of the material [Eq. (34)]. Fixing the frequency as $f=6.81$ and 12.75 GHz, we calculated the PCR as functions of θ and ϕ and depicted the patterns in Figs. 4(b) and 4(c), respectively. We find that the PCR cannot reach 1 in oblique angle incidence case. For $f=6.81$ GHz, we find that the value of ϕ to realize a maximum PCR increases toward 90° as θ increases, indicating that at glancing incidence we can rotate \vec{H} toward \hat{y} to maximize the polarization conversion effect. An opposite behavior of ϕ was found for another resonance [see Fig. 4(c)] since the resonances at $f=6.8$ GHz and $f=12.71$ GHz belong to different directions. In fact, we find that all these features are kept in the examples studied subsequently, so that we will not repeat the discussions there.

B. Scatterings by anisotropic metamaterial slabs

Although the single-interface model is intuitive, it is not quite realistic in practice. In this section, we consider the EM wave scatterings by a slab of anisotropic metamaterial which is practically realizable. We adopt two examples to illustrate the applications of the 4×4 TMM and perform brute-force FDTD simulations on specifically designed samples to verify all predictions based on the 4×4 TMM.²²

The first example is a 1.6-mm-thick metamaterial slab possessing magnetic responses along two in-plane directions,²¹

$$\mu_x = 1 + \frac{15}{12.49^2 - f^2} + \frac{100}{25.73^2 - f^2},$$

$$\mu_y = 1 + \frac{10}{7.11^2 - f^2} + \frac{110}{14.8^2 - f^2} + \frac{220}{22.12^2 - f^2},$$

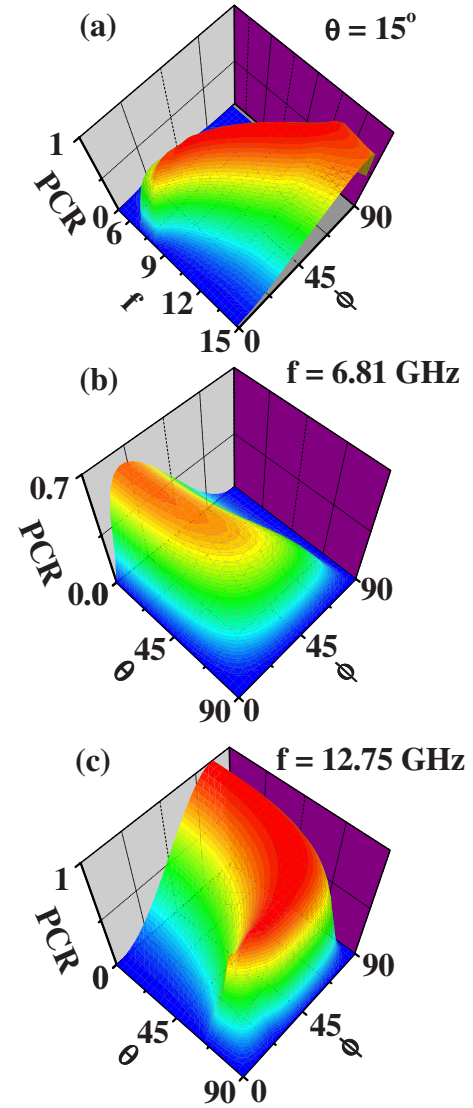


FIG. 4. (Color online) (a) PCR as a function f and ϕ with $\theta = 15^\circ$, calculated for the single-interface model. PCR as a function of θ and ϕ (b) with $f=6.81$ GHz and (c) with $f=12.75$ GHz for the single-interface model.

$$\varepsilon_x = \varepsilon_y = \varepsilon_z = \mu_z = 1. \quad (35)$$

With all material and geometrical parameters known, we employed the 4×4 TMM to study the EM wave scatterings by such a slab. Figure 5(a) shows the calculated results of r_{sp}^2 and r_{ss}^2 versus frequencies for normal incidence with $\phi = 45^\circ$. The corresponding PCRs are shown in Fig. 5(b) denoted by solid stars. We note that the spectrum calculated for a finite-thickness slab resembles that of a single-interface case (see Fig. 2) in many respects, although the details of the two spectra are quite different. For example, the reflectances, including both r_{sp}^2 and r_{ss}^2 , reach their maximum values at the two resonance frequencies, but the PCR reach their maxima at different frequencies at which r_{ss}^2 are minimized.

We next study the second example, which is a metamaterial slab of the same thickness but possesses magnetic response only along *one* direction,²¹

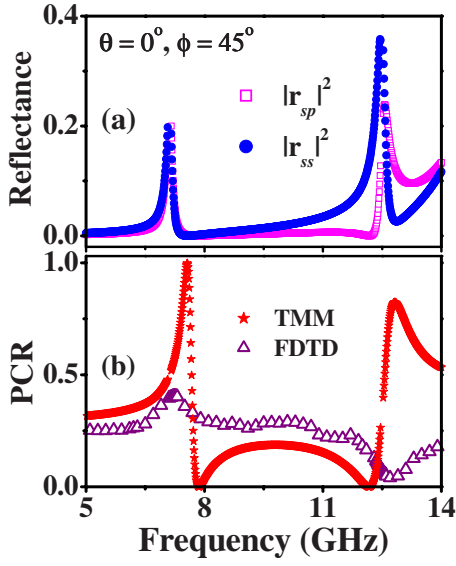


FIG. 5. (Color online) (a) For sample I, the calculated r_{sp}^2 and r_{ss}^2 as functions of frequency under the normal incidence condition with $\phi=45^\circ$. (b) PCR as a function of frequency, obtained by the 4×4 TMM (solid stars) and FDTD simulations (open triangles) for the realistic metallic structure with unit cell depicted in Fig. 7(a).

$$\mu_y = 1 + \frac{10}{7.06^2 - f^2} + \frac{110}{14.54^2 - f^2} + \frac{220}{22.56^2 - f^2},$$

$$\varepsilon_x = \varepsilon_y = \varepsilon_z = \mu_x = \mu_z = 1. \quad (36)$$

We employed the 4×4 TMM to study the scatterings by such a metamaterial slab and depicted the normal-incidence spectra of r_{sp}^2 , r_{ss}^2 , and PCR in Fig. 6, calculated with different values of ϕ . While Figs. 6(a) and 6(b) show that the spectra of r_{sp}^2 and r_{ss}^2 are quite similar to those calculated for sample I, here the PCR spectrum shown in Fig. 6(c) for sample II looks quite unusual. In particular, we find that the PCR is *solely determined by the polarization angle ϕ* , but is

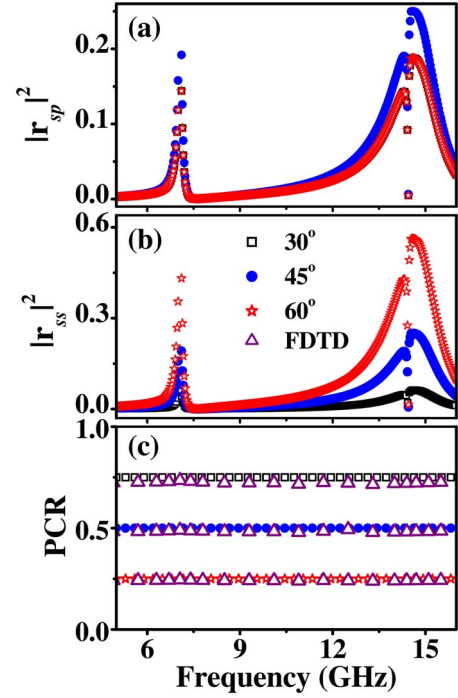


FIG. 6. (Color online) For sample II, the calculated (a) r_{sp}^2 and (b) r_{ss}^2 as functions of frequency under the normal incidence condition with different azimuth angles ϕ . (c) PCR versus frequency calculated under the normal incidence condition with different values of ϕ , obtained by the 4×4 TMM (open squares, solid circles, and open stars) and the FDTD simulation (open triangles) for the realistic metallic structure with unit cell depicted in Fig. 7(b).

independent of frequency although the metamaterial is highly dispersive [see Eq. (36)].

To understand such an intriguing phenomenon, we have derived analytical expressions for the reflection coefficients of such a slab under the normal incidence condition. After some efforts, we find that

$$r_{sp} = \frac{\sin(2\phi)[i(\varepsilon_y - \mu_x)\sqrt{\varepsilon_x}\sqrt{\mu_y}\sin(k_{z1}d)\cos(k_{z3}d) - i\sqrt{\mu_x}\sqrt{\varepsilon_y}(\varepsilon_x - \mu_y)\cos(k_{z1}d)\sin(k_{z3}d) + (\varepsilon_x\mu_x - \varepsilon_y\mu_y)\sin(k_{z1}d)\sin(k_{z3}d)]}{[-2i\sqrt{\varepsilon_y}\sqrt{\mu_x}\cos(k_{z1}d) + (\mu_x + \varepsilon_y)\sin(k_{z1}d)][-2i\sqrt{\varepsilon_x}\sqrt{\mu_y}\cos(k_{z3}d) + (\mu_y + \varepsilon_x)\sin(k_{z3}d)]}, \quad (37)$$

$$r_{ss} = \frac{2i\sqrt{\varepsilon_x}\sqrt{\mu_y}(\varepsilon_y - \mu_x)\cos^2\phi\sin(k_{z1}d)\cos(k_{z3}d) + 2i\sqrt{\mu_x}\sqrt{\varepsilon_y}(\varepsilon_x - \mu_y)\sin^2\phi\sin(k_{z3}d)\cos(k_{z1}d) + [\mu_x\mu_y - \varepsilon_x\varepsilon_y + (\varepsilon_x\mu_x - \varepsilon_y\mu_y)\cos(2\phi)]\sin(k_{z1}d)\sin(k_{z3}d)}{[-2i\sqrt{\varepsilon_y}\sqrt{\mu_x}\cos(k_{z1}d) + (\mu_x + \varepsilon_y)\sin(k_{z1}d)][-2i\sqrt{\varepsilon_x}\sqrt{\mu_y}\cos(k_{z3}d) + (\mu_y + \varepsilon_x)\sin(k_{z3}d)]}, \quad (38)$$

where $k_{z1} = (\omega/c)\sqrt{\varepsilon_x\mu_x}$ and $k_{z3} = (\omega/c)\sqrt{\varepsilon_x\mu_y}$. Although expressions (37) and (38) appear quite complicated, we can still gain a lot of physical insights via analyzing them. We see that $r_{sp} = 0$ in the cases of $\phi = 0^\circ$ and 90° due to the same reasons explained in the single-interface case. In addition, in the case of $\phi = 90^\circ$ where the property is solely determined by ε_x and μ_y , we get from Eq. (38) that

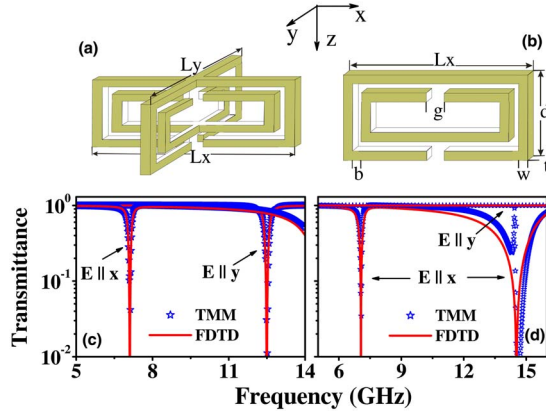


FIG. 7. (Color online) (a) Geometry of the unit cell of sample I, with parameters given by $L_x=7.4$ mm and $L_y=4$ mm. Other details are the same as sample II. (b) Geometry of the unit cell of sample I, with parameters given by $L_x=7.4$ mm, $d=1.6$ mm, $g=0.4$ mm, and $b=w=t=0.2$ mm. Transmission spectra for (c) sample I and (d) sample II for normally incident EM waves with polarizations $\vec{E}\parallel\hat{x}$ and $\vec{E}\parallel\hat{y}$, calculated by the TMM based on the effective-medium models (open stars) and the FDTD simulations for realistic structures (solids lines).

$$r_{ss} = \frac{(\mu_y - \varepsilon_x)\sin(k_{z3}d)}{[-2i\sqrt{\varepsilon_x}\sqrt{\mu_y}\cos(k_{z3}d) + (\varepsilon_x + \mu_y)\sin(k_{z3}d)]}, \quad (39)$$

which again goes back to the reflectance calculated for an isotropic slab.

The most interesting result appears when the condition $\varepsilon_x=\varepsilon_y=\mu_x\neq\mu_y$ is satisfied. In this case, while both r_{ss} and r_{sp} strongly depend on the value of μ_x , μ_y , and d , such dependences cancel each other in the expression of the PCR. Specifically, we find through straightforward calculations that

$$\text{PCR} = \frac{r_{sp}^2}{r_{ss}^2 + r_{sp}^2} = \frac{\sin^2(2\phi)}{4\sin^4\phi + \sin^2(2\phi)} = \cos^2\phi \quad (40)$$

in the case of $\phi\neq 0^\circ$. We note that the PCR cannot be defined in the case of $\phi=0^\circ$.

This peculiar property explains the intriguing behaviors of the PCR as shown in Fig. 6(c) since the material properties of sample II [$\varepsilon_x=\varepsilon_y=\mu_x=1$, see Eq. (36)] obviously satisfy the condition $\varepsilon_x=\varepsilon_y=\mu_x\neq\mu_y$. This intriguing behavior could find some applications in reality, in case that one wants to get a broad band polarization manipulation effect in practice.

FDTD simulations²³ were performed to verify these theoretical predictions obtained with the 4×4 TMM. With the help of FDTD simulations, we have designed two realistic metallic structures that exhibit the same material responses, as shown in Eqs. (35) and (36). As depicted in Figs. 7(a) and 7(b), the unit cell of sample I is composed by two split-ring resonators⁵ (SRR) of different sizes, which are perpendicular to each other, while that of sample II consists of only one single SRR. Repeat the unit cells along the $x(y)$ direction with periodicity 8 mm (5 mm), we get two 1.6-mm-thick slabs which correspond to the two samples specified by Eqs.

(35) and (36). The EM wave normal transmission spectra through the two samples were calculated through the FDTD simulations, and results were shown by solid lines in Figs. 7(c) and 7(d) for two independent polarizations ($\vec{E}\parallel\hat{x}$ and $\vec{E}\parallel\hat{y}$). We find excellent agreements between the spectra calculated by the FDTD simulations (solid lines) and by the TMM (open stars) based on the model systems represented by Eqs. (35) and (36). These excellent agreements demonstrated that our designed structures can indeed be well described by the effective medium models specified by Eqs. (35) and (36).

We then performed FDTD simulations to calculate the PCR spectra with the designed systems and showed the results as open triangles in Figs. 5(b) and 6(c), respectively.²³ Compared with the PCR spectra calculated based on the 4×4 TMM, the agreements are generally quite satisfactory. In particular, we find that the FDTD simulations *exactly* reproduced the analytical results obtained for sample II [see Eq. (40)], verifying the predictions that sample II can indeed serve as a frequency-independent polarization manipulator. However, the agreement is found to be not perfect near the resonances of sample I. We suspect that such discrepancies are caused by the finite-size effects since we have to adopt finite-sized samples in our FDTD simulations.²³

C. Scatterings by a double-layer metamaterial reflector

From the above discussions for a metamaterial slab, we find that while the PCR value can be as high as 1, the reflected signal is usually weak ($|r_{sp}|\neq 1$), indicating that the manipulation efficiency is low. The same is true for another type of metamaterial slab with $\vec{\varepsilon}$ and $\vec{\mu}$ interchanged due to the EM symmetry. The reason is simply that such single-layer slabs are usually not *totally* reflective for EM waves with arbitrary incidence angles and polarizations.

The double-layer reflector proposed in Ref. 13, consisting of a metamaterial slab and a perfect reflecting metal sheet, can be employed to remedy this problem. With the metal sheet on the back, the entire structure is always totally reflective for EM waves, independent of their incidence angles and polarizations. Meanwhile, the anisotropic metamaterial layer placed on top of the metal sheet still possesses the polarization manipulation functionalities. In Ref. 13, we have discussed several interesting phenomena related to such double-layer reflectors, including the complete polarization conversion, generalizations of arbitrary polarization states (linear, circular, and elliptical), etc. In this paper, we further study another interesting phenomenon—we show that it is possible to rotate the polarization direction of a linearly polarized incident EM wave by an *arbitrary* angle through reflections with such a double-plate reflector. We note that the same polarization angle rotation effect can be achieved as light travels across a magnetic-optical medium based on the well known Faraday effect,²⁴ but the Faraday effect requires a bulk medium while our reflector can be made very thin compared with wavelength. We now describe our results in details.

Rewriting the reflection coefficients as $r_{ss}=|r_{ss}|e^{i\varphi_s}$ and $r_{sp}=|r_{sp}|e^{i\varphi_p}$, we get the reflected waves as

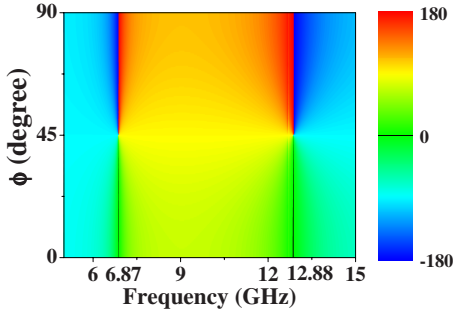


FIG. 8. (Color online) For the double-plate reflector model $\Delta\varphi_{sp}$ as functions of frequency and the azimuth angle ϕ calculated with the 4×4 TMM under the normal incident condition.

$$\vec{E}_r(\vec{r}, t) = [|r_{ss}| e^{i\Delta\varphi_{sp}} \hat{e}_s + |r_{sp}| \hat{e}_p] e^{i\varphi_p} e^{-i(\vec{k}_r \cdot \vec{r} - \omega t)}, \quad (41)$$

where the incident wave is assumed to be s polarized, \vec{k}_r is the wave vector of the reflected wave, and $\Delta\varphi_{sp} = \varphi_s - \varphi_p$ denotes the relative phase between the s - and p -polarized modes inside the reflected beam. One can easily find from Eq. (41) that the reflected wave still takes a linear polarization if the condition

$$\Delta\varphi_{sp} = 0^\circ \text{ or } 180^\circ \quad (42)$$

is fulfilled, but the polarization direction is rotated by an angle

$$\Delta\Theta = \tan^{-1}(|r_{sp}|/|r_{ss}|) \quad (43)$$

as compared to that of the original wave. When the condition PCR=1 is reached implying that $|r_{ss}|=0$, we get $\Delta\Theta=90^\circ$, indicating that the original s polarization has been completely changed to the p polarization after reflection.²⁵

To illustrate how condition (42) is met, we performed numerical calculations with the 4×4 TMM on a model system consisting of a 1.3-mm-thick anisotropic metamaterial layer with

$$\mu_{xx} = 1 + \frac{70}{12.71^2 - f^2}, \quad \mu_{yy} = 1 + \frac{22}{6.80^2 - f^2}, \quad \mu_{zz} = 1, \quad (44)$$

$$\varepsilon_{xx} = \varepsilon_{yy} = \varepsilon_{zz} = 1$$

put on top of a perfect metal sheet, which is the same model system studied in Ref. 13. Again, first consider the normal incidence case. Depicted in Fig. 8 is the calculated value of $\Delta\varphi_{sp}$ as functions of frequency and the azimuth angle ϕ . We find that the condition ($\Delta\varphi_{sp}=0^\circ$ or 180°) is satisfied at two frequencies, 6.87 and 12.88 GHz, independent of the parameter ϕ . This fact indicates that the reflected wave still takes a linear polarization at these two frequencies. For the case of oblique angle of incidence ($\theta \neq 0^\circ$), we have performed extensive numerical computations and found that condition (42) can still be met at the vicinities of the two frequencies, 6.87 and 12.88 GHz.

We then choose one of those two frequencies to quantitatively study the rotation angle $\Delta\Theta$ based on Eq. (43). Setting $f=6.87$ GHz, we calculated $|r_{sp}|$ and $\Delta\Theta$ as functions of θ and ϕ and drew the results in Figs. 9(a) and 9(b). We find

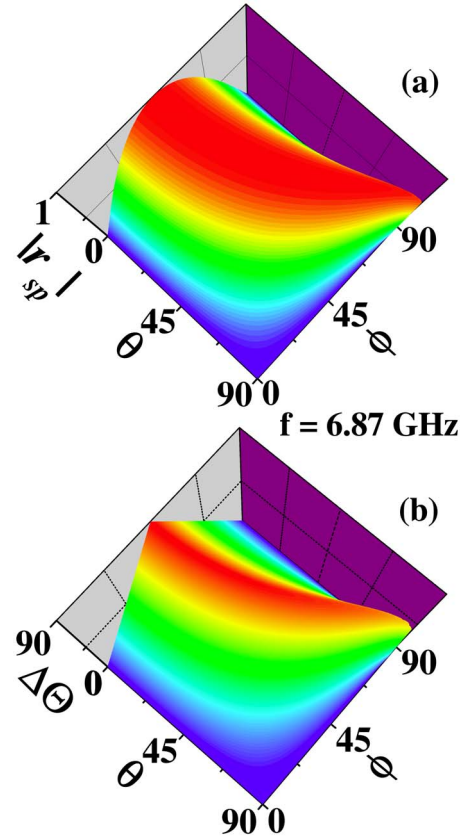


FIG. 9. (Color online) For the double-plate reflector model, values of (a) $|r_{sp}|$ and (b) $\Delta\Theta$ as functions of θ and ϕ calculated with the 4×4 TMM setting $f=6.87$ GHz.

that the pattern for $\Delta\Theta$ resembles that of $|r_{sp}|$ very much, and both of them are very complicated functions of the incidence angle specified by θ and ϕ . The most important observation is that an *arbitrary* rotation angle $\Delta\Theta$ can be obtained via adjusting the incidence direction, or equivalently speaking, via rotating the reflector appropriately. This fact indicates that we can *freely* rotate the polarization direction of a linearly polarized light by using our metamaterial reflector. This is remarkable. Although the similar polarization-rotation effect can be achieved based on the Faraday effect,²⁴ a thick medium is usually required to achieve a large rotation angle and also the efficiency is relatively low. In contrast, here our reflector is much thinner than wavelength and the efficiency is 100%.

Although the pattern of $\Delta\Theta \sim \theta, \phi$ appears quite complicated, we can derive an analytical formula for $\Delta\Theta$ in the case of normal incidence ($\theta=0^\circ$), with which many new understandings can be gained. In such a case, the incident s -polarized EM wave can be written as

$$\vec{E}_{in}(\vec{r}, t) = (-\sin \phi \hat{x} + \cos \phi \hat{y}) e^{-i(\omega z/c - \omega t)},$$

$$\vec{H}_{in}(\vec{r}, t) = (-\cos \phi \hat{x} - \sin \phi \hat{y}) e^{-i(\omega z/c - \omega t)}. \quad (45)$$

A unique property in such a situation is that the EM wave can be separated as two independent linearly polarized waves as

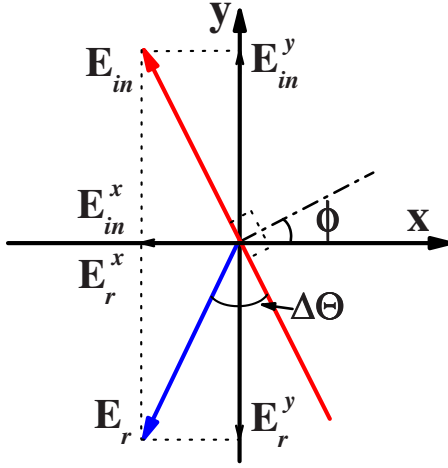


FIG. 10. (Color online) Schematic picture showing relationships among the \vec{E}_{in} vector of the incident wave, the \vec{E}_r vector of the reflected wave, and the polarization rotation angle $\Delta\Theta$, when an EM wave normally strikes on the double-plate metamaterial reflector.

$$\begin{pmatrix} \vec{E}_{in}(\vec{r}, t) \\ \vec{H}_{in}(\vec{r}, t) \end{pmatrix} = -\sin\phi \begin{pmatrix} \hat{x} \\ \hat{y} \end{pmatrix} e^{-i(\omega z/c - \omega t)} + \cos\phi \begin{pmatrix} \hat{y} \\ -\hat{x} \end{pmatrix} e^{-i(\omega z/c - \omega t)}. \quad (46)$$

For each of these two linearly polarized waves, the reflection coefficients, denoted by r_x and r_y , could take different values. Since the Maxwell equations are linear ones, we find that the reflected wave must be

$$\vec{E}_r(\vec{r}, t) = (-r_x \sin\phi \hat{x} + r_y \cos\phi \hat{y}) e^{i(\omega z/c + \omega t)}. \quad (47)$$

With a perfect-metal slab on the back, our double-layer reflector is *always totally reflecting*; that is to say, the amplitudes of the reflection coefficients r_x and r_y are always absolutely 1 but their phases could be different. Therefore, when the condition

$$r_x/r_y = -1 \quad (48)$$

is satisfied, the reflected wave still takes a linear polarization.²⁶ As condition (48) is satisfied, the \mathbf{E} vector of the reflected wave would be $\vec{E}_r \sim -\sin\phi \hat{x} - \cos\phi \hat{y}$. As schematically shown in Fig. 10, such an \mathbf{E} vector has been rotated by an angle

$$\Delta\Theta = \begin{cases} 2\phi & (0^\circ < \phi \leq 45^\circ) \\ 180^\circ - 2\phi & (45^\circ < \phi < 90^\circ) \end{cases} \quad (49)$$

with respect to that of the incident wave, $\vec{E}_{in} \sim -\sin\phi \hat{x} + \cos\phi \hat{y}$. Equation (49) thus provides us a rigorous and analytical formula to calculate the polarization rotation angle under the normal incidence condition. Indeed, the $\Delta\Theta \sim \phi$ relation calculated by the 4×4 TMM is shown by solid stars in Fig. 11, which is in excellent agreement with the analytical relation [Eq. (49)] represented by a solid line.

Again, these theoretical predictions were successfully verified by FDTD simulations on realistic structures. As we

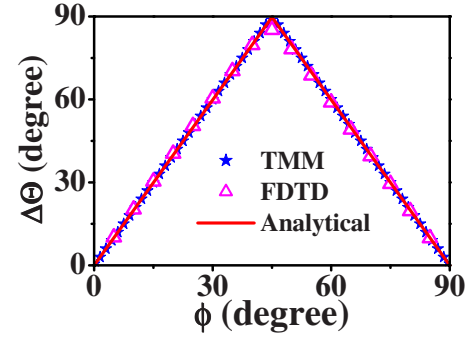


FIG. 11. (Color online) The polarization rotation angle $\Delta\Theta$ as a function of ϕ , calculated under the normal incidence condition by the 4×4 TMM (solid stars) on the model system, analytical relation [Eq. (49)] (solid line), and the FDTD simulations (open triangles) on the realistic system.

have designed in Ref. 13, a realistic metallic sandwich structure (see Fig. 1 of Ref. 13) for the model system, we then performed FDTD simulations on that realistic metallic structure to study the polarization rotation effect under the normal incidence condition. The FDTD calculated results of $\Delta\Theta$ are shown in Fig. 11 as a function of the polarization angle ϕ , represented by open triangles. We find perfect agreements between the FDTD simulations and the model TMM results, as well as the analytical relation [Eq. (49)].

While the model we studied here is assumed to exhibit magnetic response only, we emphasize that the polarization manipulation effect is not strictly tied to such kind of materials. The only requirement is that the reflection phases of the designed system should be different for two independently polarized EM waves. In fact, we found that the polarization rotation effect can still be realized if the anisotropic magnetic capping material is replaced by an appropriately designed anisotropic left-handed metamaterial whose permittivity and permeability are both negative.

IV. CONCLUSIONS

In summary, we have established a generalized 4×4 transfer-matrix method to study the scatterings of EM waves by layered anisotropic metamaterials, with incident waves taking arbitrary incidence angles and polarizations. As the illustrations, we have employed the method to study the EM wave transmission and/or reflections for three different systems, namely, an anisotropic metamaterial interface, an anisotropic metamaterial slab, and a double-plate metamaterial reflector. The obtained results show that we could manipulate EM wave polarizations freely through reflections by such anisotropic metamaterial reflectors. In particular, we show that it is possible to achieve a broadband polarization manipulation effect using a specifically designed metamaterial slab, even if the material forming the slab is highly frequency dispersive. In addition, we show it is possible to rotate the polarization direction of a linearly polarized EM wave by an arbitrary angle using a planar reflector of thickness much less than wavelength, in contrast to the conventional Faraday effect requiring a bulk medium. Finite-

difference-time-domain simulations on realistic structures are performed to successfully verify all theoretical predictions.

ACKNOWLEDGMENTS

This work was supported by the National Basic Research Program of China (Nos. 2004CB719800 and 2006CB921701), the NSFC (Nos. 10504003 and 60725417), Fok Ying Tung Education Foundation, MOE of China (No. B06011), and PCSIRT.

APPENDIX: TRANSFER-MATRIX FOR SPECIAL CASES

When EM wave propagates in an isotropic medium or in an anisotropic medium but with \mathbf{E} or \mathbf{H} field polarized along one of the optical axes, mathematical singularities of the type 0/0 arise for the unit vectors \hat{e}_σ defined by Eqs. (5)–(7). The reason is that the solutions of k_z are degenerate in such cases ($k_{z1}=k_{z3}$) so that the unit vectors \hat{e}_σ cannot be determined unambiguously by k_z as we did in Eqs. (5)–(7) and thus we have to define them explicitly. In consistency with the conventional notation, we define the \mathbf{E} field unit vector $\hat{e}_s(\vec{k})$ for the s polarization as

$$\hat{e}_s(\vec{k}) = (-k_y\hat{x} + k_x\hat{y})/k_\parallel, \quad (\text{A1})$$

with $k_\parallel = \sqrt{k_x^2 + k_y^2}$, and that for the p polarization as

$$\hat{e}_p(\vec{k}) = \hat{e}_s(\vec{k}) \times \vec{k}/k = (k_x k_z \hat{x} + k_y k_z \hat{y} - k_\parallel^2 \hat{z})/k k_\parallel. \quad (\text{A2})$$

For \mathbf{H} fields, we find that

$$\hat{h}_s(\vec{k}) = \frac{1}{\omega\mu} [\vec{k} \times \hat{e}_s(\vec{k})] = \frac{1}{\omega\mu k_\parallel} (-k_x k_z \hat{x} - k_y k_z \hat{y} + k_\parallel^2 \hat{z}), \quad (\text{A3})$$

$$\hat{h}_p(\vec{k}) = \frac{1}{\omega\mu} [\vec{k} \times \hat{e}_p(\vec{k})] = \frac{k}{\omega\mu k_\parallel} (-k_y \hat{x} + k_x \hat{y}). \quad (\text{A4})$$

The matrix D_n can be written as

$$D_n = \begin{pmatrix} \frac{k_x^{(n)}}{k_\parallel^{(n)}} & \frac{k_x^{(n)}}{k_\parallel^{(n)}} & \frac{k_y^{(n)} k_z^{(n)}}{k_\parallel^{(n)} k_\parallel^{(n)}} & -\frac{k_y^{(n)} k_z^{(n)}}{k_\parallel^{(n)} k_\parallel^{(n)}} \\ -\frac{k_x^{(n)} k_z^{(n)}}{\omega\mu^{(n)} k_\parallel^{(n)}} & \frac{k_x^{(n)} k_z^{(n)}}{\omega\mu^{(n)} k_\parallel^{(n)}} & -\frac{k_y^{(n)} k_z^{(n)}}{\omega\mu^{(n)} k_\parallel^{(n)}} & -\frac{k_y^{(n)} k_z^{(n)}}{\omega\mu^{(n)} k_\parallel^{(n)}} \\ \frac{k_y^{(n)} k_z^{(n)}}{\omega\mu^{(n)} k_\parallel^{(n)}} & \frac{k_y^{(n)} k_z^{(n)}}{\omega\mu^{(n)} k_\parallel^{(n)}} & \frac{k_x^{(n)} k_z^{(n)}}{\omega\mu^{(n)} k_\parallel^{(n)}} & \frac{k_x^{(n)} k_z^{(n)}}{\omega\mu^{(n)} k_\parallel^{(n)}} \\ -\frac{k_y^{(n)}}{k_\parallel^{(n)}} & -\frac{k_y^{(n)}}{k_\parallel^{(n)}} & \frac{k_x^{(n)} k_z^{(n)}}{k_\parallel^{(n)} k_\parallel^{(n)}} & -\frac{k_x^{(n)} k_z^{(n)}}{k_\parallel^{(n)} k_\parallel^{(n)}} \end{pmatrix}. \quad (\text{A5})$$

In the case of $k_x = k_\parallel$ ($k_y = 0$), the matrix D_n becomes automatically block diagonalized and is given by

$$D_n = \begin{pmatrix} 1 & 1 & & \\ -\frac{k_z^{(n)}}{\omega\mu^{(n)}} & \frac{k_z^{(n)}}{\omega\mu^{(n)}} & 0 & \\ & 0 & \frac{k_x^{(n)}}{\omega\mu^{(n)}} & \frac{k_x^{(n)}}{\omega\mu^{(n)}} \\ & & \frac{k_z^{(n)}}{k_\parallel^{(n)}} & -\frac{k_z^{(n)}}{k_\parallel^{(n)}} \end{pmatrix}. \quad (\text{A6})$$

The transfer matrix $M_{n+1,n}$ is then given by

$$M_{n+1,n} = D_{n+1}^{-1} D_n = \frac{1}{2} \begin{pmatrix} 1 + \frac{k_z^{(n)} \mu^{(n+1)}}{k_z^{(n+1)} \mu^{(n)}} & 1 - \frac{k_z^{(n)} \mu^{(n+1)}}{k_z^{(n+1)} \mu^{(n)}} & & \\ & & 0 & \\ 1 - \frac{k_z^{(n)} \mu^{(n+1)}}{k_z^{(n+1)} \mu^{(n)}} & 1 + \frac{k_z^{(n)} \mu^{(n+1)}}{k_z^{(n+1)} \mu^{(n)}} & & \\ & & 0 & \\ & & & \frac{k^{(n)} \mu^{(n+1)}}{k^{(n+1)} \mu^{(n)}} + \frac{k_z^{(n)} k^{(n+1)}}{k_z^{(n+1)} k^{(n)}} & \frac{k^{(n)} \mu^{(n+1)}}{k^{(n+1)} \mu^{(n)}} - \frac{k_z^{(n)} k^{(n+1)}}{k_z^{(n+1)} k^{(n)}} \\ & & & \frac{k^{(n)} \mu^{(n+1)}}{k^{(n+1)} \mu^{(n)}} - \frac{k_z^{(n)} k^{(n+1)}}{k_z^{(n+1)} k^{(n)}} & \frac{k^{(n)} \mu^{(n+1)}}{k^{(n+1)} \mu^{(n)}} + \frac{k_z^{(n)} k^{(n+1)}}{k_z^{(n+1)} k^{(n)}} \end{pmatrix} = \begin{pmatrix} M_{n+1,n}^s & 0 \\ 0 & M_{n+1,n}^p \end{pmatrix}, \quad (\text{A7})$$

with $M_{n+1,n}^s$ and $M_{n+1,n}^p$ the transfer matrices for s and p modes in a conventional case.¹⁶

*Corresponding author; phzhou@fudan.edu.cn

¹D. R. Smith, J. B. Pendry, and M. C. K. Wiltshire, *Science* **305**, 788 (2004).

²R. A. Shelby, D. R. Smith, and S. Schultz, *Science* **292**, 77

(2001).

³Jensen Li, Lei Zhou, C. T. Chan, and P. Sheng, *Phys. Rev. Lett.* **90**, 083901 (2003).

⁴J. B. Pendry, *Phys. Rev. Lett.* **85**, 3966 (2000).

- ⁵J. B. Pendry, A. J. Holden, D. J. Robbins, and W. J. Stewart, *IEEE Trans. Microwave Theory Tech.* **47**, 2075 (1999).
- ⁶D. R. Smith, Willie J. Padilla, D. C. Vier, S. C. Nemat-Nasser, and S. Schultz, *Phys. Rev. Lett.* **84**, 4184 (2000).
- ⁷D. R. Smith and D. Schurig, *Phys. Rev. Lett.* **90**, 077405 (2003).
- ⁸L. Zhou, C. T. Chan, and P. Sheng, *Phys. Rev. B* **68**, 115424 (2003).
- ⁹Shulin Sun, Xueqin Huang, and Lei Zhou, *Phys. Rev. E* **75**, 066602 (2007).
- ¹⁰Liangbin Hu and S. T. Chui, *Phys. Rev. B* **66**, 085108 (2002).
- ¹¹Qiang Cheng and Tie Jun Cui, *Appl. Phys. Lett.* **87**, 174102 (2005).
- ¹²Tian Jiang, Junming Zhao, and Yijun Feng, *J. Phys. D* **40**, 1821 (2007).
- ¹³Jiaming Hao, Yu. Yuan, Lixin Ran, Tao Jiang, Jin Au Kong, C. T. Chan, and Lei Zhou, *Phys. Rev. Lett.* **99**, 063908 (2007).
- ¹⁴Max Born and Emil Wolf, *Principles of Optics* (Cambridge University Press, Cambridge, England, 1999).
- ¹⁵A. Papakostas, A. Potts, D. M. Bagnall, S. L. Prosvirnin, H. J. Coles, and N. I. Zheludev, *Phys. Rev. Lett.* **90**, 107404 (2003).
- ¹⁶Pochi Yeh, *Optical Wave in Layered Media* (Wiley, New York, 1988).
- ¹⁷See, e.g., K. Busch, C. T. Chan, and C. M. Soukoulis, in *Photonic Band Gap Materials*, edited by C. M. Soukoulis (Kluwer, Dordrecht, 1996).
- ¹⁸K. S. Yee, *IEEE Trans. Antennas Propag.* **14**, 302 (1966).
- ¹⁹Lei Zhou, Weijia Wen, C. T. Chan, and P. Sheng, *Phys. Rev. Lett.* **94**, 243905 (2005).
- ²⁰For the case of $\theta \neq 0^\circ$, the electric field of s -polarized wave has $\vec{E} \parallel \hat{e}_s = (-\sin \phi \hat{x} + \cos \phi \hat{y})$ and the p -polarized wave has $\vec{E} \parallel \hat{e}_p = (\cos \theta \cos \phi \hat{x} + \cos \theta \sin \phi \hat{y} - \sin \theta \hat{z})$.
- ²¹For the sake of simplifications, we have neglected the material losses in all the models adopted in this paper [see Eqs. (34)–(36) and (44)]. We found from numerical calculations that all qualitative conclusions drawn in this paper remain unchanged after adding losses to the materials. In particular, we found that while the reflection coefficients r_{ss} and r_{sp} are sensitive to the material losses, the PCR value is relatively robust against the losses.
- ²²While the models we adopted here are assumed to exhibit magnetic responses only, we note that the same results can be obtained if we exchange $\vec{\mu}$ with $\vec{\epsilon}$ ($\mu_x \leftrightarrow \epsilon_y$ and $\mu_y \leftrightarrow \epsilon_x$) due to the EM symmetry.
- ²³Simulations were performed using the package CONCERTO 4.0, developed by Vector Fields Limited, England, (2004). In our simulations, a basic cell sized $0.2 \times 0.2 \times 0.5 \text{ mm}^3$ is adopted to discretize the space. Finer submeshes were adopted in space regions where strong inhomogeneity exists. When calculating the PCR spectra in FDTD simulations, we adopted a sample sized $40 \times 45 \text{ mm}^2$ for case I and a sample sized $56 \times 54 \text{ mm}^2$ for case II.
- ²⁴L. D. Landau, E. M. Lifshitz, and L. P. Pitaevskii, *Electrodynamics of Continuous Media* (Butterworth-Heinemann Ltd., London, England, 1984).
- ²⁵We note that the physics of the present polarization rotation effect is essentially the same as that for the ellipsometry technique. See, e.g., *Handbook of Optics*, edited by W. G. Driscoll and W. Vaughan (McGraw-Hill, New York, 1978), Sec. 10. However, we emphasize that the present introduction of both ϵ and μ freedoms using metamaterials offers more possibilities to efficiently control the polarization states of electromagnetic waves.
- ²⁶We note that condition (48) is applicable only to the case of normal incidence, but condition (42) is valid in a general situation.